BIOLOGICAL CRYSTALLOGRAPHY
ISSN 1399-0047

# Structure of ginseng major latex-like protein 151 and its proposed lysophosphatidic acid-binding mechanism

**Sun-Hye Choi,[a]‡ Myoung-Ki Hong,[b]‡ Hyeon-Joong Kim,[a] Nayeon Ryoo,[c] Hyewhon Rhim,[c] Seung-Yeol Nah[a]* and Lin-Woo Kang[b,d]***

[a]Ginsentology Research Laboratory and Department of Physiology and Bio/Molecular Informatics Center, College of Veterinary Medicine, Konkuk University, Seoul 143-701, Republic of Korea, [b]Department of Biological Sciences, Konkuk University, 1 Hwayang-dong, Gwangjin-gu, Seoul 143-701, Republic of Korea, [c]Center for Neuroscience, Korea Institute of Science and Technology, 9-1 Hawholgok-dong, Sungbok-gu, Seoul 139-791, Republic of Korea, and [d]Protein and Chemical Inc., Korea Industry and Academy Cooperation Building 14, 120 Neungdong-ro, Gwangjin-gu, Seoul 143-701, Republic of Korea. *Correspondence e-mail: synah@konkuk.ac.kr, lkang@konkuk.ac.kr

Received 28 October 2014
Accepted 6 February 2015

Edited by P. Langan, Oak Ridge National Laboratory, USA

‡ These authors contributed equally to this work.

**Keywords:** *Panax ginseng*; ginseng major latex-like protein 151; plant LPA-binding protein; G protein-coupled LPA receptor.

**PDB references**: ginseng major latex-like protein 151, 4reh; 4rei; 4rej

**Supporting information**: this article has supporting information at journals.iucr.org/d

Lysophosphatidic acid (LPA) is a phospholipid growth factor with myriad effects on biological systems. LPA is usually present bound to animal plasma proteins such as albumin or gelsolin. When LPA complexes with plasma proteins, it binds to its cognate receptors with higher affinity than when it is free. Recently, gintonin from ginseng was found to bind to LPA and to activate mammalian LPA receptors. Gintonin contains two components: ginseng major latex-like protein 151 (GLP) and ginseng ribonuclease-like storage protein. Here, the crystal structure of GLP is reported, which belongs to the plant Bet v 1 superfamily, and a model is proposed for how GLP binds LPA. Amino-acid residues of GLP recognizing LPA were identified using site-directed mutagenesis and isothermal titration calorimetry. The resulting GLP mutants were used to study the activation of LPA receptor-dependent signalling pathways. In contrast to wild-type GLP, the H147A mutant did not bind LPA, elicit intracellular $Ca^{2+}$ transients in neuronal cells or activate $Ca^{2+}$-dependent $Cl^-$ channels in *Xenopus* oocytes. Based on these results, a mechanism by which GLP recognizes LPA and its requirement to activate G protein-coupled LPA receptors to elicit diverse biological responses were proposed.

## 1. Introduction

Lysophosphatidic acids (LPAs) are simple, ubiquitous and well characterized phospholipid derivatives (Choi *et al.*, 2010). LPAs exert their effects by activating G-protein coupled receptors known as LPA receptors 1–6. The primary action of LPAs is to elicit transient changes in the cytosolic calcium concentration $[Ca^{2+}]_i$ and to induce cell proliferation, differentiation, morphological changes, migration and survival through the activation of LPA receptors (Choi & Chun, 2013). These diverse LPA receptor-related cellular functions are coupled to activities such as brain development in the nervous system, angiogenesis in the vascular system, embryo implantation and spermatogenesis in the reproductive system and wound healing (Choi & Chun, 2013). In animals, various extracellular and intracellular proteins are used to deliver LPAs to cellular organelles or various target organs. LPAs bind intracellular fatty acid-binding proteins to transport mitochondrial LPA to microsomes for phosphatidic acid synthesis (Pagès *et al.*, 2001). LPAs also bind extracellular albumin and gelsolin with high affinity (Goetzl, 2001). These two proteins are necessary for the maintenance of various

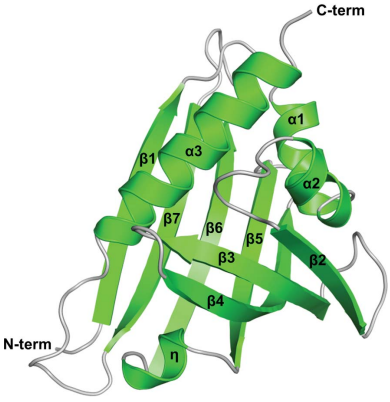

biological activities of LPA and for the avoidance of LPA degradation by plasma lysophospholipases (Tigyi & Miledi, 1992).

In plants, LPAs play structural roles as main intermediate components in phosphatidic acid synthesis. Phosphatidic acids are converted into phospholipids and glycerolipids for cellular membranes in plants (Bourgis *et al.*, 1999; Choi *et al.*, 1985*a*,*b*; Kim *et al.*, 1988). Plants also contain LPA-binding proteins. However, the functions of plant LPA-binding proteins have been less studied than those of animals (Webber & Hajra, 1992). Recently, a unique bioactive LPA–protein complex was found and named gintonin. Gintonin consists of LPAs such as LPA $C_{18:2}$, LPA $C_{18:1}$ and LPA $C_{16:0}$, as well as ginseng major latex-like protein 151 (GLP) and ginseng ribonuclease-like storage protein (GSP) (Hwang, Shin, Choi *et al.*, 2012). In particular, gintonin is a novel high-affinity ligand for mammalian G protein-coupled LPA receptors (Hwang, Shin, Choi *et al.*, 2012).

As a protein component of gintonin, GLP belongs to the Bet v 1 protein superfamily, the members of which contain a hydrophobic ligand-binding site at the central position and a glycine-rich loop, called a P-loop, which is thought to bind nucleotides (Saraste *et al.*, 1990). GLP has three potential *N*-glycosylation sites: Thr35, Ser61 and Ser126 (Sun, Nam *et al.*, 2010). Although GSP is homologous to plant ribonuclease, GSP does not have ribonuclease activity (Kim, Kweon *et al.*, 2004). GSP expression in ginseng root varies seasonally and it acts as a storage protein during the vegetative stage in ginseng (Kim, Kweon *et al.*, 2004). Thus, GLP, rather than GSP, was proposed to play the main role in binding LPA in gintonin and in the gintonin-mediated activation of LPA receptors. Similarly, human MLN64, a member of the Bet v 1 protein superfamily, has a START (StAR-related lipid-transfer) domain and plays a role as a steroid carrier (Reitz *et al.*, 2008). The size and properties of the hydrophobic ligand-binding cavity determine the binding of various compounds (Neudecker *et al.*, 2001; Marković-Housley *et al.*, 2003; Pasternak *et al.*, 2006). Thus far, LPA-bound gintonin has been thought to act as a novel extracellular ligand to trigger LPA receptor-mediated signalling pathways (Hwang, Shin, Choi *et al.*, 2012). However, it is unknown how GLP, the protein component of gintonin, binds to or interacts with LPA or how LPA is delivered to LPA receptors.

In the present study, we determined the crystal structure of GLP and investigated how GLP recognizes LPA by using site-directed mutagenesis and thermodynamic affinity measurements of wild-type and mutant GLP, which were also used for $[Ca^{2+}]_i$ transient assays in cells. Based on our results, we propose a mechanism by which GLP recognizes LPA and delivers it to G protein-coupled LPA receptors.

## 2. Materials and methods

### 2.1. Materials

LPA $C_{18:1}$ and LPA $C_{18:2}$ were purchased from Avanti Polar Lipids (Alabaster, Alabama, USA) and Echelon Biosciences Inc. (Salt Lake City, Utah, USA). GLP (EU939308.1) was cloned into the pET-15b vector by ATGen Co. Ltd (Seongnam, Republic of Korea). The $Ca^{2+}$-imaging dyes fura-2-acetoxymethyl ester (fura-2-AM) and Pluronic F-127 were purchased from Molecular Probes (Eugene, Oregon, USA). All other reagents were purchased from Sigma–Aldrich (St Louis, Missouri, USA).

### 2.2. Expression and purification of GLP

A polymerase chain reaction (PCR) product containing the *GLP* open reading frame was digested using NdeI and XhoI and then ligated into pET-15b. The resulting vector was then transformed into *Escherichia coli* BL21 (DE3) cells for protein expression. The transformed strains were grown to an absorbance of 0.5 at 600 nm in Luria–Bertani medium containing ampicillin (50 µg ml$^{-1}$) at 37°C. Protein expression was then induced by the addition of 0.5 m*M* IPTG. 5 h after induction, the cells were harvested *via* centrifugation (20 min, 6000*g*, 4°C). The pellets were resuspended in lysis buffer (20 m*M* Tris–HCl pH 8.0, 0.5 *M* NaCl, 5 m*M* imidazole) and then lysed by sonication. Following centrifugation at 13 000*g* at 4°C for 15 min, the supernatant was applied onto Ni–NTA resin (Qiagen) pre-equilibrated with lysis buffer. The resin with bound protein was washed with buffer (50 m*M* NaCl, 20 m*M* Tris–HCl pH 8.0, 10 m*M* imidazole) to remove weakly bound contaminants and then eluted from the column with elution buffer (50 m*M* NaCl, 20 m*M* Tris–HCl pH 8.0, 250 m*M* imidazole). The eluate was then dialyzed with 20 m*M* Tris–HCl pH 8.0 to remove the imidazole. The His tag was cleaved from the protein using a thrombin cleavage kit (Sigma). Following a second round of dialysis with 20 m*M* Tris–HCl pH 8.0, the cleaved protein was concentrated using a centrifugal filter tube (Millipore).

### 2.3. GLP–LPA binding study

For the binding assay, LPA $C_{18:1}$ (175 µ*M*) and the purified wild-type or mutant GLP (140 µ*M*) were combined in a solution consisting of 150 m*M* NaCl, 20 m*M* Tris–HCl pH 7.0. The mixture was incubated at 25°C for 1 h and then loaded onto a Superdex 75 10/300 size-exclusion column for chromatography to separate the bound and unbound forms; 1 ml was collected per fraction.

### 2.4. Crystallization, data collection and structure determination

Crystallization conditions were determined by the sitting-drop vapour-diffusion method using a Hydra II eDrop automated pipetting system (Matrix Technologies Ltd, Stafford, England) at 14°C (287 K). The drops consisted of 0.5 µl protein solution (7 mg ml$^{-1}$ in 20 m*M* Tris–HCl pH 8.0) and 0.5 µl reservoir solution. The solution was equilibrated against 70 µl reservoir solution at 14°C (287 K). The initial crystallization conditions tested were derived from the Wizard Precipitant Synergy kit (Emerald Bio), the Index kit (Hampton Research) and the Crystal Screen kit (Hampton Research). After two weeks, crystal 1 grew in a condition from

the Wizard Precipitant Synergy kit [condition No. 37; 5%(*v*/*v*) 2-propanol, 2 *M* ammonium citrate/citric acid pH 6.5], crystal 2 gew in a condition from the Index kit (condition No. 23; 2.1 *M* DL-malic acid pH 7.0) and crystal 3 grew in a condition from the Crystal Screen kit (condition No. 2-28; 1.6 *M* sodium citrate tribasic dehydrate pH 6.5). The initial crystals were optimized *via* the sitting-drop vapour-diffusion method using a CombiClover Plate (Emerald Bio). The crystals were cryoprotected in the reservoir solution and then mounted on the goniometer in a stream of cold nitrogen at 100 K.

X-ray diffraction data were collected to a resolution of 1.5 Å from the GLP crystals at 100 K using an ADSC Q315r detector on beamline 5C SB II at the Pohang Light Source in the Republic of Korea and using a Dectris Pilatus 2M-F detector on beamline BL-1A at the Photon Factory in Japan. The diffraction data were integrated and scaled using the *DENZO* and *SCALEPACK* crystallographic data-reduction routines (Otwinowski & Minor, 1997). The crystals belonged to a trigonal space group ($P3_121$), with unit-cell parameters $a = b = 61.8$, $c = 91.2$ Å. Matthews coefficient analysis indicated that the asymmetric unit consisted of a single molecule ($V_M$ = 2.96 Å$^3$ Da$^{-1}$), giving a solvent content of 58.5%. The structure was determined by the molecular-replacement method with *MOLREP* (Vagin & Teplyakov, 2010) using a model generated by protein structure prediction by the *Robetta* server (Kim, Chivian *et al.*, 2004) and the solution structure of major latex protein 28 (MLP28) from *Arabidopsis thaliana* (PDB entry 2i9y; 45% sequence identity; Lytle *et al.*, 2009). The models were further built manually using *Coot* (Emsley & Cowtan, 2004) and refined using *REFMAC*5 (Murshudov *et al.*, 2011). The resulting data and refinement statistics are provided in Table 1. Structural figures were prepared using *PyMOL* (DeLano, 2002).

**Table 1**
Data-collection and refinement statistics.

Values in parentheses are for the highest resolution shell.

| | Crystal 1 | Crystal 2 | Crystal 3 |
|---|---|---|---|
| Data collection | | | |
| X-ray source† | 5C, PLS | 5C, PLS | BL-1A, KEK |
| Space group | $P3_121$ | $P3_121$ | $P3_121$ |
| Unit-cell parameters | | | |
| $a = b$ (Å) | 61.8 | 61.9 | 61.8 |
| $c$ (Å) | 91.2 | 91.9 | 91.4 |
| $\alpha = \beta$ (°) | 90 | 90 | 90 |
| $\gamma$ (°) | 120 | 120 | 9120 |
| Resolution (Å) | 50.00–1.50 (1.53–1.50) | 50.00–1.50 (1.53–1.50) | 50.00–1.70 (1.76–1.70) |
| Total reflections | 347013 | 334110 | 440727 |
| Unique reflections | 32837 | 33189 | 23046 |
| Completeness (%) | 99.7 (100.0) | 98.6 (100.0) | 100.0 (100.0) |
| Multiplicity | 10.6 (10.8) | 10.1 (10.7) | 19.1 (19.8) |
| $\langle I/\sigma(I)\rangle$ | 62.0 (7.7) | 62.2 (10.4) | 55.2 (5.7) |
| $R_{merge}$ (%) | 4.8 (40.4) | 5.9 (36.7) | 5.6 (46.7) |
| Refinement | | | |
| Resolution (Å) | 29.27–1.50 | 26.82–1.50 | 30.90–1.70 |
| No. of reflections | 31128 | 31458 | 21829 |
| $R_{work}/R_{free}$ (%) | 18.0/21.6 | 19.6/22.4 | 18.9/22.1 |
| No. of atoms | | | |
| Protein | 1201 | 1151 | 1164 |
| Ligand | — | 11 | — |
| Water | 161 | 143 | 105 |
| *B* factors (Å$^2$) | | | |
| Protein | 20.7 | 21.5 | 23.1 |
| Ligand | — | 34.2 | — |
| Water | 30.6 | 32.5 | 30.2 |
| R.m.s. deviations | | | |
| Bond lengths (Å) | 0.031 | 0.031 | 0.023 |
| Bond angles (°) | 2.64 | 2.77 | 2.13 |
| Ramachandran plot (%) | | | |
| Favoured | 97.2 | 97.9 | 97.9 |
| Allowed | 2.8 | 2.1 | 2.1 |
| Disallowed | 0 | 0 | 0 |
| PDB code | 4reh | 4rei | 4rej |

† BL-1A, KEK: beamline BL-1A, Photon Factory, Japan; 5C, PLS: beamline 5C SB II, Pohang Light Source, Republic of Korea.

### 2.5. Isothermal titration calorimetry

Isothermal titration calorimetry (ITC) was conducted using a Nano ITC calorimeter (TA Instruments, New Castle, Delaware, USA) with a cell volume of 190 µl at 25°C. A 50 µl injection syringe was loaded with 1.2 m*M* LPA $C_{18:2}$ solution. After temperature equilibration, 2 µl aliquots were injected into ITC sample cells containing wild-type GLP, the H30A mutant, the H147A mutant or the H148A mutant (all at 240 µ*M*) at 4 min intervals. The contents of the sample cell were stirred at 400 rev min$^{-1}$ throughout the experiment. Both GLP and LPA were dissolved in 10 m*M* Tris–HCl pH 7.5. The heat of dilution from injecting the ligand into the buffer was subtracted before the fitting process. Data analysis was performed using the *NanoAnalyze* software (TA Instruments) and the data were fitted to an independent model.

### 2.6. Site-directed mutagenesis of putative phosphate-binding residues in GLP

For site-directed mutagenesis, recombinant PCR was used to replace His29, His30, His147 and His148 with alanine. The single amino-acid substitutions were made using the QuikChange XL Site-Directed Mutagenesis Kit (Stratagene, La Jolla, California, USA) along with *Pfu* DNA polymerase and sense and antisense primers encoding the desired mutations. Overlap extension of the target domain by sequential PCR was carried out according to the manufacturer's protocol. The final PCR products were transformed into *E. coli* DH5α cells. The transformants were screened by PCR and the inserts in the resulting vectors were confirmed by sequencing.

### 2.7. Oocyte preparation for transformation

South African clawed frogs (*Xenopus laevis*) were obtained from Xenopus I (Ann Arbor, Michigan, USA). Their care and handling were in accordance with the highest standards of institutional guidelines. Oocytes were isolated from frogs under anesthaesia with an aerated solution of 3-aminobenzoic acid ethyl ester. The oocytes were then separated by treatment with collagenase and agitation for 2 h in a $Ca^{2+}$-free medium consisting of 82.5 m*M* NaCl, 2 m*M* KCl, 1 m*M* $MgCl_2$, 5 m*M* HEPES pH 7.5, 2.5 m*M* sodium pyruvate, 100 units ml$^{-1}$ penicillin and 100 µg ml$^{-1}$ streptomycin. Stage V–VI oocytes were collected and stored in ND96 (96 m*M* NaCl, 2 m*M* KCl, 1 m*M* $MgCl_2$, 1.8 m*M* $CaCl_2$, 5 m*M* HEPES pH 7.5)

supplemented with 0.5 m*M* theophylline and 50 µg ml$^{-1}$ gentamicin. This oocyte-containing solution was maintained at 18°C with continuous gentle shaking and was changed daily.

### 2.8. Electrophysiological recording conditions

Two-electrode voltage-clamp recordings were obtained from individual oocytes placed in a small Plexiglas net chamber (0.5 ml) that was continuously superfused with ND96. The microelectrodes were filled with 3 m*M* KCl and had a resistance of 0.2–0.7 MΩ. The electrophysiological experiments were performed at room temperature using an Oocyte Clamp Amplifier (OC-725C; Warner Instruments, Hamden, Connecticut, USA). Linear leak and capacitance currents were corrected with a leak-subtraction procedure. $LPA_{18:1}$ complexed with wild-type or mutant GLP was applied to the oocytes by bath perfusion.

### 2.9. Primary neural precursor cell culture

Embryonic day 14.5 embryos were dissected from pregnant C57BL/6 mice and the hippocampi were isolated in calcium-free and magnesium-free Hank's Balanced Salt Solution (HBSS). The resulting cells were plated at 2.5 × 10$^4$ cells cm$^{-2}$ into 10 cm dishes coated with 15 µg ml$^{-1}$ poly-L-ornithine and 1 µg ml$^{-1}$ fibronectin (Invitrogen) containing N2 medium supplemented with B27 (Invitrogen). The dishes were then incubated at 37°C in 95% air, 5% $CO_2$. Basic fibroblast growth factor (bFGF; 20 ng ml$^{-1}$; R&D Systems) and epidermal growth factor (EGF; 20 ng ml$^{-1}$; R&D Systems) were added daily to expand the population of neural precursors and the medium was changed every other day. Cells at 80% confluency were passaged and maintained at 6 × 10$^4$ cells cm$^{-2}$ in B27-supplemented N2 medium containing bFGF and EGF. These subcultured progenitors were subsequently induced to differentiate by the withdrawal of bFGF and EGF and were then kept in differentiation medium (neurobasal medium supplemented with B27) for 3–5 d, with the medium changed on day 3.

### 2.10. Intracellular $Ca^{2+}$-imaging techniques and measurement of $[Ca^{2+}]_i$ changes

Fura-2-AM was used as the fluorescent $Ca^{2+}$ indicator. Cells were incubated for 40–60 min at room temperature with 5 µ*M* fura-2-AM and 0.001% Pluronic F-127 in a HEPES-buffered solution (150 m*M* NaCl, 5 m*M* KCl, 1 m*M* $MgCl_2$, 2 m*M* $CaCl_2$, 10 m*M* glucose, 10 m*M* HEPES pH 7.4). The cells were then illuminated using a xenon arc lamp. Excitation wavelengths (340 or 380 nm) were selected by a computer-controlled filter wheel. Emitted light was reflected through a 515 nm long-pass filter to a cooled frame-transfer CCD camera, and ratios of emitted fluorescence were calculated using a digital fluorescence analyzer. All data were collected and analyzed using an FDSS6000 system and the related software (Hamamatsu Photonics).

### 2.11. Statistical analysis

All values were presented as the mean ± the standard error of the mean (SEM). The significance of differences between mean wild-type and mutant values was determined using Student's t-test, where $P < 0.05$ was considered to be statistically significant.

## 3. Results

### 3.1. Overall structure of GLP

GLP from *Panax ginseng* was crystallized in the trigonal space group $P3_121$. The asymmetric unit consisted of a single molecule. The crystal structure of GLP was determined by molecular replacement using major latex protein 28 (MLP28; Lytle *et al.*, 2009) as the search model and was refined at a resolution of 1.5 Å (Table 1). The GLP molecule is composed of 151 residues (residues 2–150 are visible in the electron-density map). The overall structure of GLP shows the conserved helix–grip fold that is characteristic of members of the Bet v 1 superfamily. The GLP fold consists of three $\alpha$-helices and a curved seven-stranded antiparallel $\beta$-sheet wrapped around the long C-terminal helix $\alpha$3 (residues 131–148). The two shorter helices, $\alpha$1 (residues 17–26) and $\alpha$2 (residues 28–34), are located between the $\beta$1 and $\beta$2 strands. The glycine-rich loop (residues 47–53) was positioned between the $\beta$2 and $\beta$3 strands (Fig. 1).

Crystal structures were determined from crystals obtained under three different crystallization conditions: crystal 1 [5%(*v*/*v*) 2-propanol, 2 *M* ammonium citrate/citric acid pH 6.5], crystal 2 (2.1 *M* DL-malic acid pH 7.0) and crystal 3 (1.6 *M*

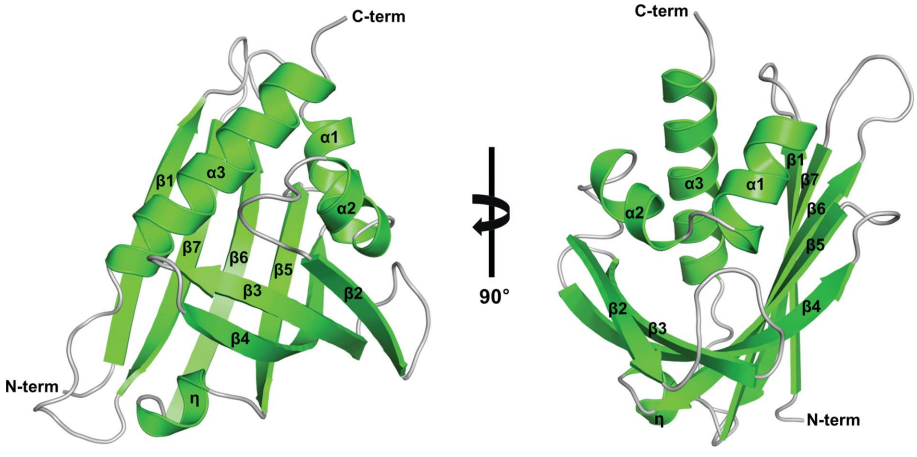


**Figure 1**
Structure of ginseng major latex-like protein 151 from *P. ginseng*. The ribbon diagram shows the overall fold of the structure, with $\alpha$-helices and $\beta$-strands shown as green coils and arrows, respectively. Loop regions are coloured grey. All helices and strands, including those at the N- and C-termini, are labelled. The ribbon representation is shown in two orientations related by a 90° rotation.

sodium citrate tribasic dehydrate pH 6.5). The three crystal structures showed the same overall conformation except for the flexible loop region between the $\beta$6 and $\beta$7 strands (residues 107–112). The root-mean-square deviation (r.m.s.d.) between the crystal 1 and crystal 2 structures was 0.32 Å over 146 aligned $C^{\alpha}$ atoms and that between the crystal 1 and crystal 3 structures was 0.29 Å over 148 aligned $C^{\alpha}$ atoms. The crystal 1 structure displayed all residues, including the loop at residues 107–112. However, parts of the loop in crystal 2 (residues 109–111) and crystal 3 (residue 111) were missing owing to flexibility.

### 3.2. Structural comparison with other Bet v 1 superfamily members

The GLP structure was compared with the structures of homologous Bet v 1 superfamily members, including the solution structure of MLP28 from *A. thaliana* (PDB entry 2i9y; 45% sequence identity), the crystal structure of Act d 11 from kiwifruit (PDB entry 4ihr; 50% sequence identity) and the crystal structure of Bet v 1 from the birch *Betula verrucosa* (PDB entry 1bv1; 15% sequence identity).

MLP28 has the conserved helix–grip fold found in all Bet v 1 superfamily members (Lytle *et al.*, 2009). However, the structures of GLP and MLP28 have substantial differences in the $\alpha$2 helix and the $\beta$2 strand. The r.m.s.d. value between the GLP and the MLP28 structures was 2.87 Å over 124 $C^{\alpha}$ atoms of GLP. The secondary structures of GLP $\alpha$2 and $\beta$2 were replaced by a long flexible loop in MLP28, despite having high sequence identity (residues 28–47; 75% sequence identity; Fig. 2*a*). In the region of the $\alpha$2 helix and the loop between the $\alpha$2 helix and the $\beta$2 strand, the Pro32, Asn33, Ile34, Thr35 and Ala37 residues in GLP were substituted in MLP28 by serine, lysine, alanine, serine and glycine, respectively. In the $\beta$2 strand these residues were completely conserved (Fig. 2*c*). It is quite interesting that although all residues from the $\alpha$2 helix to the $\beta$2 strand, including the linking loop region, were strictly conserved in terms of hydrophobicity between GLP and MLP28, the two secondary structures were completely different.

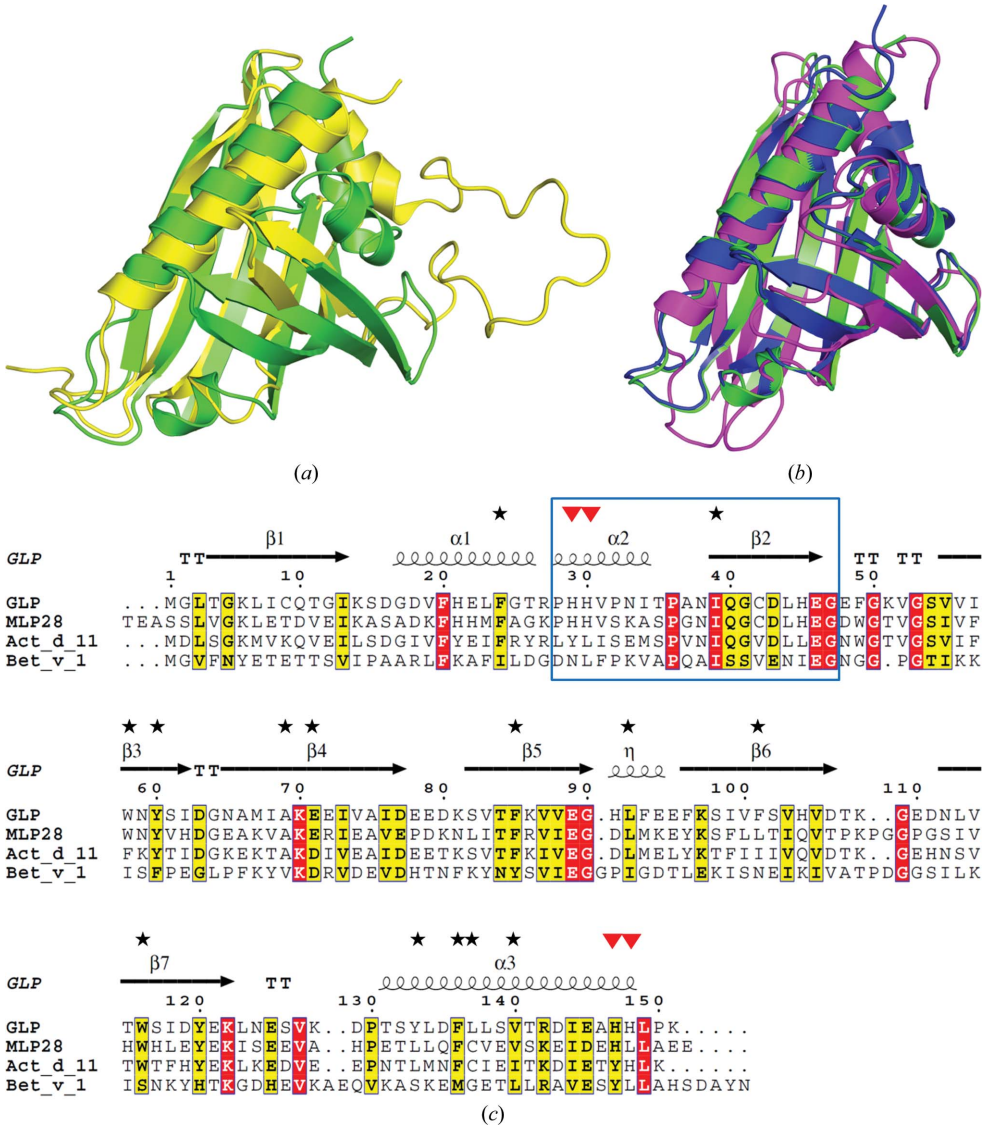


**Figure 2**
Structural comparison between ginseng major latex-like protein 151 and other Bet v 1 superfamily members. (*a*) Superposition of ginseng major latex-like protein 151 (GLP; green) and the lowest energy major latex protein 28 (MLP28) conformer (yellow). (*b*) Superposition of GLP (green), Act d 11 (blue) and Bet v 1 (magenta). (*c*) Structure-based sequence alignment of GLP with other Bet v 1 superfamily members. Conserved residues are shown as white letters in red boxes. Conservative substitutions are placed in yellow boxes. Starred residues represent the hydrophobic pocket sequence. Residues marked with a red triangle represent the mutated residues in this study. $\eta$ indicates a $3_{10}$-helix. TT indicates $\beta$-turns. The long flexible loop in MLP28 is indicated with a blue box.

Act d 11 is the kiwifruit allergen also known as kirola (Chruszcz *et al.*, 2013). The structural conformations of GLP and Act d 11 were similar (Fig. 2*b*). The r.m.s.d. between the GLP and Act d 11 structures was only 0.70 Å over 146 $C^{\alpha}$ atoms of GLP. Bet v 1, the major birch pollen allergen, was the first member of the Bet v 1 superfamily for which the structure was characterized (Gajhede *et al.*, 1996). The structure of GLP was similar to that of Bet v 1, despite the low sequence identity between the two proteins (Fig. 2*b*). The r.m.s.d. between

the GLP and Bet v 1 structures was 1.94 Å over 137 $C^{\alpha}$ atoms of GLP. Glu46 in GLP is conserved in all of the homologous proteins, including Bet v 1, and the glutamate residue is important for causing allergy *via* direct binding to IgE (Hurlburt *et al.*, 2013).

### 3.3. The hydrophobic ligand-binding cavity in GLP

All Bet v 1 superfamily members have a central hydrophobic cavity. All three GLP structures also contained a hydrophobic cavity in which there was electron density for an unidentified ligand. Most of the protein residues covering the cavity were hydrophobic except for Glu71, and there was no solvent-accessible surface. The overall shapes of the unidentified electron densities were similar in the three crystal structures (Figs. 3*a*–3*c*). The bound ligand could have come from solutions used in the protein-purification or crystallization steps or from cellular metabolic compounds. The purified GLP protein solution used for crystallization was extracted with 1-butanol to separate the bound unidentified ligand. Mass spectrometry (MS/MS) was then used to identify the ligand most likely to fit in the electron density by searching

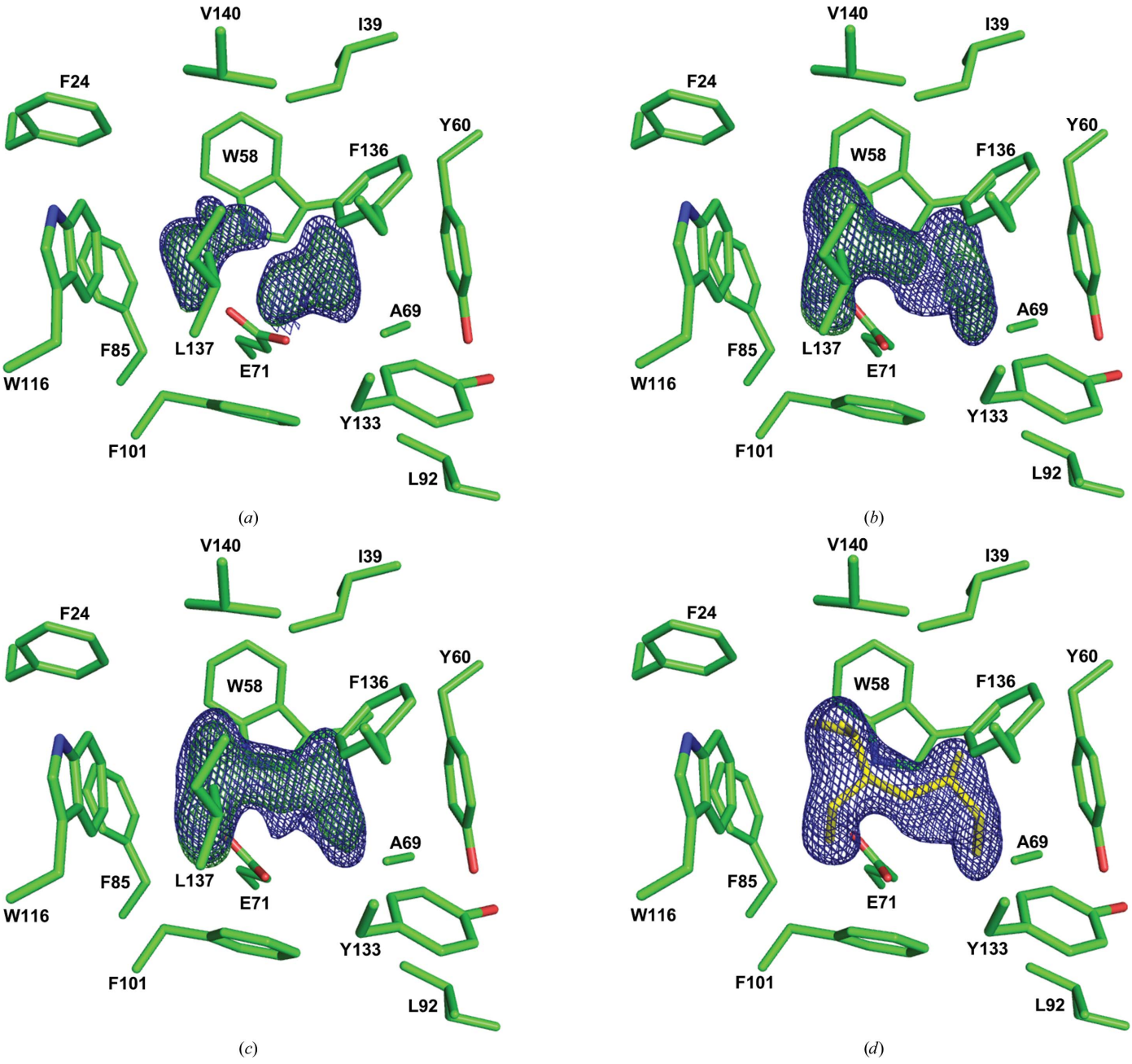


**Figure 3**
The residues forming the central cavity were determined using the $2F_o - F_c$ map (contoured at 1.0$\sigma$; blue) or the $F_o - F_c$ map (contoured at 3.0$\sigma$; green). The data indicate the presence of an unknown ligand. (*a*) Crystal 1. (*b*) Crystal 2. (*c*) Crystal 3. (*d*) Crystal 2 with 2,5-dimethyl-3-ethylheptane.

**Table 2**
Thermodynamic parameters for lysophosphatidic acid $C_{18:2}$ complexed with wild-type (WT) or mutant ginseng major latex-like protein 151.

Titrations were performed at 25°C. The Gibbs free energy ($\Delta G$) and entropy ($\Delta S$) were calculated using the equations $\Delta G = -RT\ln K$ and $\Delta S = (\Delta H - \Delta G)/T$, respectively.

| Enzyme | $n$ | $K_d$ ($\mu M$) | $\Delta G$ (kJ mol$^{-1}$) | $T\Delta S$ (kJ mol$^{-1}$) | $\Delta H$ (kJ mol$^{-1}$) |
|---|---|---|---|---|---|
| WT | 0.98 | 6.57 | −29.58 | 4.62 | −24.96 |
| H30A | 0.99 | 6.60 | −29.57 | −5.50 | −35.07 |
| H147A | N/D† | N/D | N/D | N/D | N/D |
| H148A | 0.99 | 4.50 | −30.51 | 22.37 | −8.14 |

† N/D, not determined.

the mass-spectrometry compound database library. However, no compound matching the electron-density map was found.

The cavity-forming hydrophobic residues in GLP are Phe24, Ile39, Trp58, Tyr60, Ala69, Glu71, Phe85, Leu92, Phe101, Trp116, Tyr133, Phe136, Leu137 and Val140. As mentioned above, all of these residues are hydrophobic except for Glu71. The hydrophobic pocket residues of GLP were very well conserved in homologous proteins such as MLP28, Act d 11 and Bet v 1, with similarly hydrophobic residues (Fig. 2*c*). In addition, the only hydrophilic residue, Glu71, was conserved or replaced by aspartate, which is also hydrophilic.

The volumes of the central cavities in the homologous proteins were calculated using *Computed Atlas of Surface Topography of proteins* (*CASTp*; Dundas *et al.*, 2006). The central hydrophobic cavity of GLP was slightly smaller than that of Act d 11: the volumes of the cavities in GLP and Act d 11 were approximately 316 and 399 Å$^3$, respectively. The cavities in MLP28 (2193 Å$^3$) and Bet v 1 (1527 Å$^3$) were significantly larger (*i.e.* sevenfold and fivefold larger, respectively) than that in GLP.

Diverse chemical compounds can bind in the hydrophobic cavities of Bet v 1 superfamily members. Previous work indicated that the bound compounds were usually hydrophobic containing aromatic rings such as an indole (*e.g.* tryptamine) or steroids (Reitz *et al.*, 2008; Mogensen *et al.*, 2002). However, the geometry of the hydrophobic cavity in GLP implies the presence of an aliphatic rather than an aromatic ring compound. Using a high-resolution electron-density map, we built and fitted an artificial molecule into the unidentified electron density. Because the electron-density information obtained by X-ray crystallography could not identify the atom type in the density, the molecule was built as the simplest hydrocarbon molecule. An aliphatic 2,5-dimethyl-3-ethyl-heptane molecule was fitted into the density to represent a putative ligand for the central cavity (Fig. 3*d*). LPA was much larger than the central cavity or the artificially built ligand, and no channel existed connecting the solvent to the central cavity that could accommodate the long hydrophobic fatty-acid chain in LPA. Therefore, in order for LPA to bind to the central cavity, some part of GLP should undergo conformational changes to form a channel to the central hydrophobic pocket.

### 3.4. Identification of putative LPA-recognizing amino acids in GLP *via* isothermal titration calorimetry

Purified GLP formed a stable complex with LPA $C_{18:1}$, as confirmed by size-exclusion chromatography (Pyo *et al.*, 2011). We used circular-dichroism spectroscopy to study the possible conformational changes of GLP upon binding LPA. However, no noticeable conformational change was observed. This

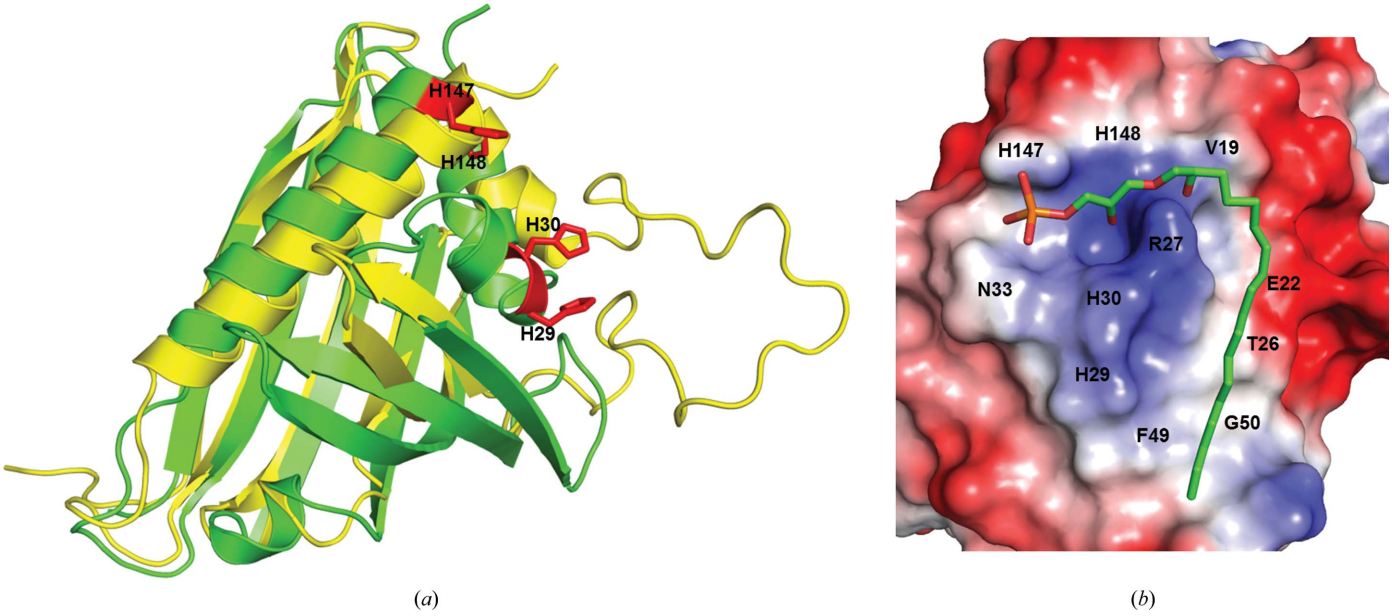


**Figure 4**
Recognition of lysophosphatidic acid $C_{18:2}$ by ginseng major latex-like protein 151. (*a*) Superposition of ginseng major latex-like protein 151 (GLP; green) and the lowest energy major latex protein 28 conformer (yellow). The mutated residues in GLP are represented by red sticks. (*b*) The electrostatic molecular surface of GLP modelled with LPA $C_{18:2}$ in close conformation. The positions of the residues that recognize LPA $C_{18:2}$ are labelled.

result suggests that LPA binds to the surface of GLP rather than through the central hydrophobic cavity. We next attempted to obtain LPA-bound or LPA analogue-bound co-crystal structures using all three available crystallization conditions and some new conditions. However, the crystals obtained by soaking or co-crystallization with LPA or LPA analogues showed no distinct extra density for the soaked ligand.

Instead, we used biochemical methods to study LPA recognition by GLP. We searched for residues that could bind the negatively charged phosphate moiety in LPA. Four candidate histidine residues next to the glycine-rich P-loop, which is thought to be the nucleotide phosphate-binding motif, were identified and individually replaced by alanine (Fig. 4*a*). The His147 and His148 residues are in the $\alpha$3 helix and His29 and His30 are in the $\alpha$2 helix. The binding affinities between the wild-type or mutant GLP and LPA $C_{18:2}$ were measured by ITC. The thermodynamic parameters for the interactions are summarized in Table 2. The His147 mutant (H147A) completely lost its affinity for LPA. This result shows that

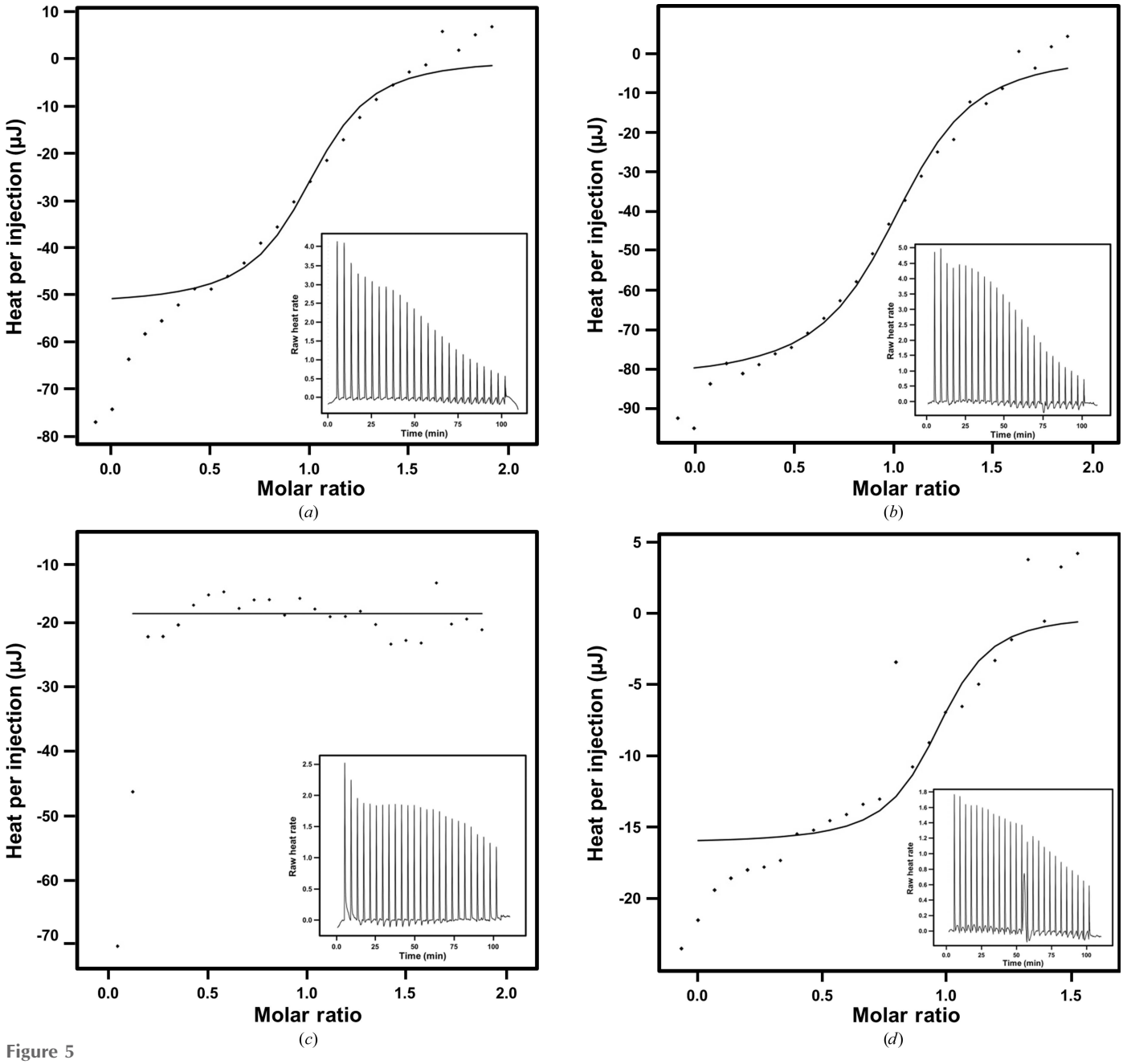


**Figure 5**
Isothermal titration calorimetry analysis of the interactions of lysophosphatidic acid $C_{18:2}$ with wild-type and mutant ginseng major latex-like protein 151. Both the isotherms and the raw data are presented. The graphs show that heat is produced after each injection and that the signal is diminished when the protein becomes saturated with ligand. (*a*) Direct titration of lysophosphatidic acid (LPA) $C_{18:2}$ into wild-type ginseng major latex-like protein 151 (GLP) and mutant versions of GLP in which (*b*) His30, (*c*) His147 or (*d*) His148 were replaced by alanine. The fitting of the data yielded the thermodynamic parameters listed in Table 2.

His147 plays a key role in the binding of GLP to LPA (Figs. 5*a*–5*d*). Based on the recognition of the LPA phosphate by His147, a model of LPA-bound GLP was proposed in which the hydrophobic long fatty-acid chain of LPA was bound on the hydrophobic surface along the $\alpha$1 helix to the P-loop of GLP (Fig. 4*b*). We also measured the binding affinity between wild-type GLP and the LPA analogues cyclic phosphatidic acid and alkylglycerophosphate. Neither of these LPA analogues showed any affinity for GLP (Supplementary Fig. S1).

### 3.5. LPA $C_{18:1}$ bound to wild-type (but not H147A) GLP induces $[Ca^{2+}]_i$ transients in mouse hippocampal neural precursor cells

Levels of intracellular $Ca^{2+}$ signalling, $[Ca^{2+}]_i$, were measured in mouse hippocampal neural precursor cells (NPCs), which mainly express the LPA1 receptor (Sun, Kim *et al.*, 2010). The $[Ca^{2+}]_i$ was induced by activation of the G protein-coupled LPA receptor with LPA $C_{18:1}$ in complex with wild-type or mutant GLP. LPA $C_{18:1}$ in complex with wild-type GLP (GLP–LPA $C_{18:1}$) induced $[Ca^{2+}]_i$ transients. In addition, LPA $C_{18:1}$ bound to the His29-to-alanine (H29A) mutant or the His-30-to-alanine (H30A) mutant also induced $[Ca^{2+}]_i$ transients. However, the H147A mutant GLP–LPA $C_{18:1}$ complex did not induce $[Ca^{2+}]_i$ transients (Figs. 6*a* and 6*b*; $n$ = 7). In contrast, the H148A mutant GLP–LPA $C_{18:1}$ complex induced a slight increase in $Ca^{2+}$ mobilization compared with that induced by the wild-type GLP–LPA $C_{18:1}$ complex. These results show that the His147 and His148 residues in GLP play an important role in cellular $[Ca^{2+}]_i$ transients in response to LPA $C_{18:1}$.

### 3.6. LPA $C_{18:1}$ bound to wild-type (but not H147A) GLP activates an endogenous $Ca^{2+}$-activated chloride channel in *Xenopus* oocytes

$Ca^{2+}$-activated chloride channels (CaCC) are activated by G protein-coupled LPA receptors. Activation of endogenous CaCC by the GLP–LPA $C_{18:1}$ complex was measured in *Xenopus* oocytes (Kimura *et al.*, 2001) expressing the LPA1 receptor. *Xenopus* oocytes express endogenous LPA receptors and have a resting CaCC current at a −80 mV holding potential. Recombinant GLP alone had no influence on the activation of CaCC in *Xenopus* oocytes. However, wild-type GLP bound to LPA $C_{18:1}$ could activate CaCC (Figs. 7*a* and 7*b*; $n$ = 5). CaCC activation in response to LPA $C_{18:1}$ bound to mutant GLPs was then examined. Both the H29A GLP–LPA $C_{18:1}$ complex and the H30A GLP–LPA $C_{18:1}$ complex activated CaCC. However, the H147A GLP–LPA $C_{18:1}$ complex did not activate CaCC (Figs. 7*a* and 7*b*). We also observed that the extent of CaCC activation induced by the H148A GLP–LPA $C_{18:1}$ complex was less than that induced by the wild-type GLP–LPA $C_{18:1}$ complex. These results suggest that the His147 and His148 residues are important for the interaction between GLP and LPA and for activation of the LPA receptor.

### 3.7. GLP induces morphological changes in mouse hippocampal NPCs only when bound to LPA $C_{18:1}$

Activation of the LPA receptor induced morphological changes in neural cells (Yanagida *et al.*, 2007). We examined the effects of GLP alone and bound to LPA $C_{18:1}$ on morphological changes in NPCs. Treatment with GLP alone did not induce morphological changes in NPCs even after 90 min (Fig. 8*a*). However, when NPCs were treated with GLP

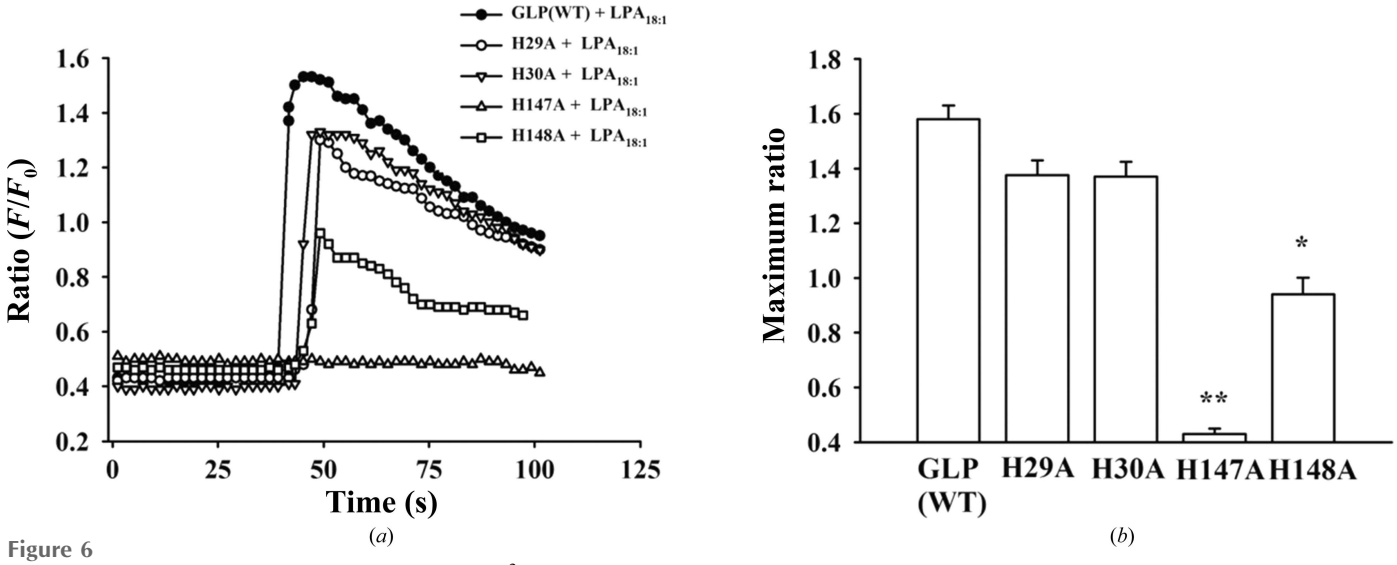


(*a*) (*b*)

**Figure 6**
Lysophosphatidic acid $C_{18:1}$ increased intracellular $Ca^{2+}$ levels when bound to ginseng major latex-like protein 151 but not when bound to a mutant version in which His147 was replaced by alanine. (*a*) Neuronal precursor cells were treated with lysophosphatidic acid (LPA) $C_{18:1}$ bound to wild-type or mutant ginseng major latex-like protein 151 (GLP). Measurements of $[Ca^{2+}]_i$ transients were performed using an FDSS6000 system. $[Ca^{2+}]_i$ transients were determined as the $F/F_0$ ratio of fluo-4-acetoxymethyl ester intensities. (*b*) Histograms showing that the maximum $F/F_0$ ratio after stimulation with the GLP–LPA complex was significantly blocked or attenuated when the GLP His147 or His148 residues were replaced by alanine (H147A and H148A, respectively) compared with when the His29 or the His30 residues were replaced by alanine (H29A and H30A, respectively) or when the GLP was the wild type [GLP(WT)]. The $Ca^{2+}$ response is represented as the maximum ratio. Data are shown as means ± SEM ($n$ = 8–10; $P < 0.01$ and $P < 0.001$ compared with the wild-type GLP–LPA $C_{18:1}$ complex are marked * and **, respectively).

bound to LPA $C_{18:1}$ the neurites of the NPCs retracted. After 90 min of treatment most of the NPCs became rounded and had no cytoplasmic extensions (Fig. 8*b*). These results show that LPA $C_{18:1}$-bound GLP affects NPC morphology.

## 4. Discussion

Because LPAs were first found in animal sources such as smooth muscle (Vogt, 1963), most studies have focused on LPA-mediated biological effects *via* LPA receptors. Although plants also contain LPAs as metabolic intermediate in *de novo* lipid synthesis (Bourgis *et al.*, 1999; Webber & Hajra, 1992), there are no reports on the roles of plant LPAs in animal systems. Recent studies report that ginseng, an oriental traditional herbal medicine, contains LPA–ginseng protein (GLP and GSP) complexes. Gintonin from ginseng specifically activates G protein-coupled LPA receptors with high affinity in animal cells (Hwang, Shin, Choi *et al.*, 2012). *In vitro* studies show that gintonin regulates a variety of $Ca^{2+}$-dependent ion channels such as $BK_{Ca}$, Kv1.2 and KCNQ $K^+$ channels, and receptors such as NMDA and $P2X_1$, *via* activation of endogenous LPA receptors (Shin *et al.*, 2012; Choi, Kim *et al.*, 2013; Choi, Lee *et al.*, 2013; Lee *et al.*, 2013; Choi *et al.*, 2014). Other studies show that gintonin exhibits anti-Alzheimer's disease effects by activating the non-amyloidogenic pathway *via* LPA receptors, and produces antimetastatic effects by inhibiting autotoxin activity (Hwang, Shin, Shin *et al.*, 2012; Hwang *et al.*, 2013). These results show that gintonin exerts its effects in animal systems *via* the activation of LPA receptors. Gintonin activates diverse LPA receptor subtypes in the order subtype 2 > subtype 5 > subtype 1 > subtype 3 > subtype 4 (Hwang, Shin, Choi *et al.*, 2012). To induce *in vitro* and *in vivo* effects, the protein components of gintonin might play an important role in LPA binding and LPA delivery to its cognate receptors.

In the current study, the crystal structure of GLP was determined. We also proposed a model of the interaction between LPA and GLP and a mechanism for the activation of LPA receptors by the GLP–LPA complex. The Bet v 1 superfamily includes pathogenesis-related class 10 proteins, cytokinin-binding proteins, MLPs and ripening-related proteins. Bet v 1 superfamily proteins are found in various fruits and vegetables and can be allergens in humans (Fernandes *et al.*, 2013). MLP is associated with fruit and flower development and pathogen defence responses in plants (Sinha *et al.*, 2014).

All homologous Bet v 1, START, RHO alpha C, PITP, CoxG and CalC domains have central hydrophobic ligand-binding cavities that are thought to bind hydrophobic ligands (Reitz *et al.*, 2008; Neudecker *et al.*, 2001; Marković-Housley *et al.*, 2003; Pasternak *et al.*, 2006; Mogensen *et al.*, 2002). The GLP structure has the 'helix–grip' fold that is well conserved in the Bet v 1 superfamily (Chruszcz *et al.*, 2013), in which the hydrophobic cavity is also conserved. Bet v 1 superfamily proteins can bind various organic compounds such as deoxycholate, brassinosteroids, cytokinin, flavonoids, zeatin and fatty acids in the hydrophobic cavity (Radauer *et al.*, 2008). The human protein MLN64 binds cholesterol in the cavity of the START domain (Radauer *et al.*, 2008).

The cavity sizes vary as much as sevenfold, from 316 $Å^3$ in GLP to 2193 $Å^3$ in MLP28. Among Bet v 1 superfamily members, Act d 11 has a structure that is similar to that of GLP (r.m.s.d. of 0.70 Å). However, the cavity size of GLP (316 $Å^3$) is smaller than that of Act d 11 (430 $Å^3$), and the unidentified ligand in the GLP cavity appears to be an aliphatic molecule rather than the aromatic ring-containing

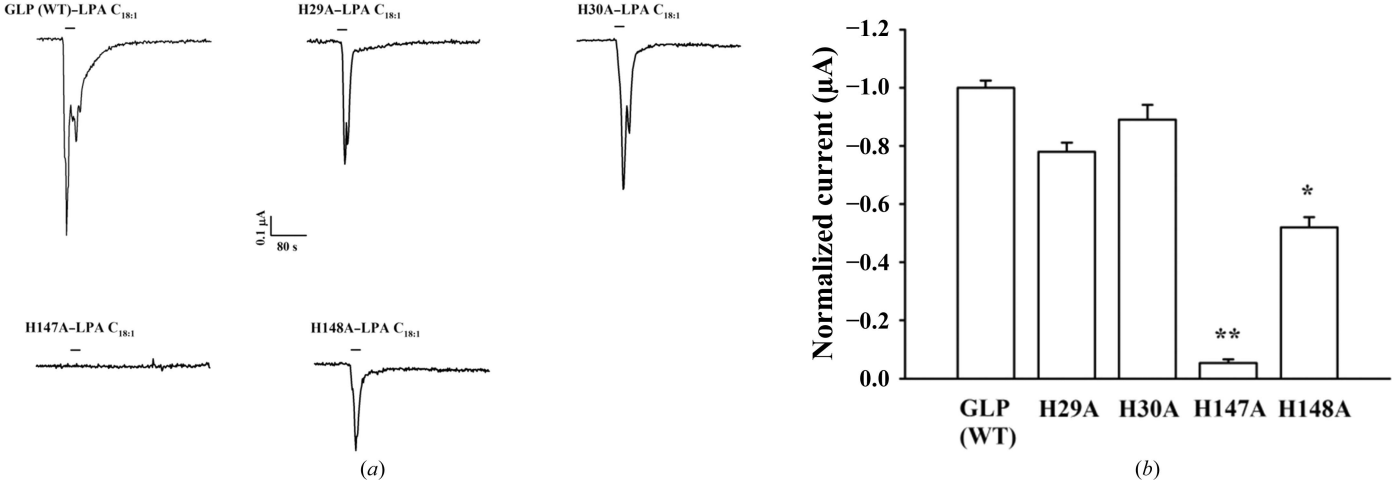


**Figure 7**
Lysophosphatidic acid $C_{18:1}$ activated endogenous $Ca^{2+}$-activated chloride channels in *Xenopus* oocytes when bound to wild-type ginseng major latex-like protein 151 but not when bound to a mutant version in which His147 was replaced by alanine. (*a*) Representative traces showing the effects of lysophosphatidic acid $C_{18:1}$ complexed with wild-type ginseng major latex-like protein 151 [GLP(WT)–LPA $C_{18:1}$] or mutant versions of GLP in which His29, His30, His147 or His148 were replaced with alanine (H29A–LPA $C_{18:1}$, H30A–LPA $C_{18:1}$, H147A–LPA $C_{18:1}$ and H148A–LPA $C_{18:1}$, respectively), on the activation of $Ca^{2+}$-activated chloride channels (CaCC). Current traces were recorded at a −80 mV holding potential at the indicated time. (*b*) Bars represent the peak inward CaCC currents on each complex. Data are shown as means ± SEM ($n = 5$ for each complex; $P < 0.01$ and $P < 0.001$ compared with the wild-type GLP-LPA $C_{18:1}$ complex are marked * and **, respectively).

molecule found in the Act d 11 cavity. When we attempted to identify the unidentified ligand by mass spectrometry, a peak was found at 119 Da. In contrast, the unidentified ligand in the Act d 11 structure had a peak at approximately 250 Da. However, we could not find a ligand with a size of 119 Da to fit in the hydrophobic electron-density map (Fig. 3).

To confirm the LPA-binding site in GLP, site-directed mutagenesis of residues that possibly interact with the phosphate group in LPA was performed. Specifically, His30, His29, His147 and His148 were mutated. Results from ITC analysis, $Ca^{2+}$ signalling and cell-morphology changes confirmed that the His147 and His148 residues play major and partial roles, respectively, in the recognition of LPA by GLP. With the H147A mutant, LPA binding was almost completely inhibited (Fig. 5*c*). In addition, the H147A mutant did not evoke $[Ca^{2+}]_i$ transients or activate CaCC (Figs. 6 and 7). These results show that the His147 residue in the $\alpha$3 helix plays an important role in LPA binding rather than the hydrophobic pocket.

The ability of GLP to bind to other LPA analogues was tested. However, two LPA analogues, cyclic phosphatidic acid and alkylglycerophosphate, showed no affinity for GLP. This implied that the recognition of LPA by GLP may be specific. We do not know whether other members of the Bet v 1 superfamily also have affinity for LPA. However, the His147 residue of GLP, which is important for LPA binding, is only conserved in the MLP28 sequence, not in Act d 11 or Bet v 1.

LPA receptors are expressed in most animal cells (Noguchi *et al.*, 2009). When bound to serum albumin or gelsolin, LPAs activate LPA receptors with a higher affinity than free LPAs (Tigyi & Miledi, 1992). Therefore, serum albumin and gelsolin were proposed to function as LPA storage and transport vehicles. Similarly, GLP could be a plant-derived LPA carrier. In the current study, we found that GLP binds to phosphate groups in LPAs mainly *via* the His147 and His148 residues located at the C-terminal $\alpha$3 helix, as arginine and lysine residues are important for gelsolin binding of the phosphate groups in LPA and $PIP_2$ (Fernandes *et al.*, 2013).

The mechanism by which LPA-bound GLP activates LPA receptors on the plasma membrane to initiate signalling cascades is interesting. GLP could deliver LPAs to nearby LPA receptors. The subsequent interactions between GLP and the LPA receptors may be direct or indirect. In our ITC experiments, the affinity between GLP and LPA was in the micromolar range. The relatively weak interactions between the hydrophobic long fatty-acid chain of LPA and the surface of GLP could help with the release of LPA from GLP. LPA receptors have a much higher affinity for LPAs, in the nanomolar range. We speculate that LPAs could be transferred and presented to LPA receptors in complex with GLP, as plasma proteins such as albumin and gelsolin are for LPA receptor activation (Goetzl *et al.*, 2000). Interestingly, the surface electron potentials of the LPA-binding side of GLP and the extracellular sides of LPA receptors are complementary, and putative glycosylation sites in GLP are not on the interaction surface (Supplementary Fig. S2). However, further studies are necessary to confirm the interactions between GLP and LPA

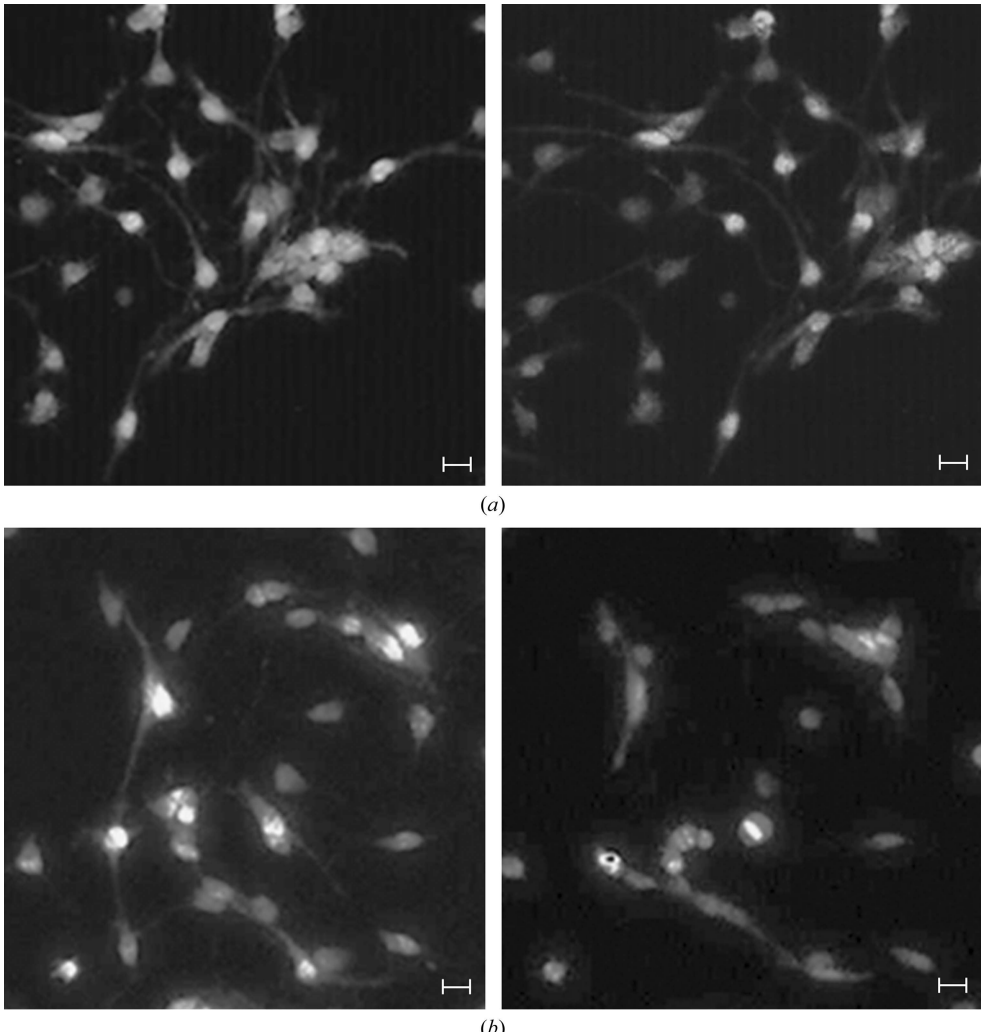

(*a*)

(*b*)

**Figure 8**
Ginseng major latex-like protein 151 induces morphological changes in neural precursor cells only when complexed with lysophosphatidic acid $C_{18:1}$. (*a*) Hippocampal neural precursor cells (NPCs) before (left) and after (right) treatment for 90 min with ginseng major latex-like protein 151. (*b*) Hippocampal NPCs before (left) and after (right) treatment for 90 min with GLP complexed with lysophosphatidic acid $C_{18:1}$. The experiments were performed as described in §2. The scale bar is 20 µm in length.

receptors. In conclusion, we propose that plant-derived GLP is an LPA-binding protein and that the GLP–LPA complex can activate LPA receptors.

## Acknowledgements

We are grateful to the staff of beamline 5C SB II at the Pohang Light Source, Republic of Korea and the staff of beamline BL-1A at the Photon Factory, Japan, for their assistance. This work was supported by the Basic Science Research Program (NRF-2014R1A1A2054538) and the Priority Research Centers Program through the National Research Foundation of Korea (NRF), which is funded by the Ministry of Education, Science and Technology (2012-0006686) and by the BK21 plus a project fund to S-YN. This work was also supported by the Basic Science Research Program through the National Research Foundation of Korea (NRF) funded by the Ministry of Education (NRF-2014R1A6A3A01057478), the 'Cooperative Research Program for Agriculture Science & Technology Development (Project No. PJ01127901)' from Rural Development Administration, Republic of Korea, and the Technology Commercialization Support Program (Project No. 113066-1), Ministry of Agriculture, Food and Rural Affairs.

## References

Bourgis, F., Kader, J. C., Barret, P., Renard, M., Robinson, C., Robinson, C., Delseny, M. & Roscoe, T. J. (1999). *Plant Physiol.* **120**, 913–922.
Choi, J. W. & Chun, J. (2013). *Biochim. Biophys. Acta*, **1831**, 20–32.
Choi, J. W., Herr, D. R., Noguchi, K., Yung, Y. C., Lee, C.-W., Mutoh, T., Lin, M.-E., Teo, S. T., Park, K. E., Mosley, A. N. & Chun, J. (2010). *Annu. Rev. Pharmacol. Toxicol.* **50**, 157–186.
Choi, K. J., Kim, M. W. & Kim, D. H. (1985*a*). *J. Ginseng Res.* **9**, 193–203.
Choi, K. J., Kim, M. W. & Kim, D. H. (1985*b*). *J. Ginseng Res.* **9**, 204–212.
Choi, S.-H., Lee, B.-H., Hwang, S.-H., Kim, H.-J., Lee, S.-M., Kim, H.-C., Rhim, H. & Nah, S.-Y. (2013). *Evid. Based Complement. Alternat. Med.* **2013**, 323709.
Choi, S.-H., Lee, B.-H., Kim, H.-J., Jung, S.-W., Kim, H.-S., Shin, H.-C., Lee, J.-H., Kim, H.-C., Rhim, H., Hwang, S.-H., Ha, T. S., Kim, H. J., Cho, H. & Nah, S.-Y. (2014). *Mol. Cells*, **37**, 656–663.
Choi, S.-H., Kim, H.-J., Kim, B.-R., Shin, T.-J., Hwang, S.-H., Lee, B.-H., Lee, S.-M., Rhim, H. & Nah, S.-Y. (2013). *Mol. Cells*, **35**, 142–150.
Chruszcz, M., Ciardiello, M. A., Osinski, T., Majorek, K. A., Giangrieco, I., Font, J., Breiteneder, H., Thalassinos, K. & Minor, W. (2013). *Mol. Immunol.* **56**, 794–803.
DeLano, W. L. (2002). *PyMOL*. http://www.pymol.org.
Dundas, J., Ouyang, Z., Tseng, J., Binkowski, A., Turpaz, Y. & Liang, J. (2006). *Nucleic Acids Res.* **34**, W116–W118.
Emsley, P. & Cowtan, K. (2004). *Acta Cryst.* D**60**, 2126–2132.
Fernandes, H., Michalska, K., Sikorski, M. & Jaskolski, M. (2013). *FEBS J.* **280**, 1169–1199.
Gajhede, M., Osmark, P., Poulsen, F. M., Ipsen, H., Larsen, J. N., Joost van Neerven, R. J., Schou, C., Løwenstein, H. & Spangfort, M. D. (1996). *Nature Struct. Biol.* **3**, 1040–1045.
Goetzl, E. J. (2001). *Prostaglandins Other Lipid Mediat.* **64**, 11–20.
Goetzl, E. J., Lee, H., Azuma, T., Stossel, T. P., Turck, C. W. & Karliner, J. S. (2000). *J. Biol. Chem.* **275**, 14573–14578.
Hurlburt, B. K., Offermann, L. R., McBride, J. K., Majorek, K. A., Maleki, S. J. & Chruszcz, M. (2013). *J. Biol. Chem.* **288**, 36890–36901.
Hwang, S. H., Lee, B.-H., Kim, H.-J., Cho, H.-J., Shin, H.-C., Im, K.-S., Choi, S.-H., Shin, T.-J., Lee, S.-M., Nam, S.-W., Kim, H.-C., Rhim, H. & Nah, S.-Y. (2013). *Int. J. Oncol.* **42**, 317–326.
Hwang, S. H., Shin, T.-J., Choi, S.-H., Cho, H.-J., Lee, B.-H., Pyo, M. K., Lee, J.-H., Kang, J., Kim, H.-J., Park, C.-W., Shin, H.-C. & Nah, S.-Y. (2012). *Mol. Cells*, **33**, 151–162.
Hwang, S. H., Shin, E.-J., Shin, T.-J., Lee, B.-H., Choi, S. -H., Kang, J., Kim, H.-J., Kwon, S.-H., Jang, C.-G., Lee, J.-H., Kim, H.-C. & Nah, S.-Y. (2012). *J. Alzheimers Dis.* **31**, 207–223.
Kim, D. E., Chivian, D. & Baker, D. (2004). *Nucleic Acids Res.* **32**, W526–W531.
Kim, S. I., Kweon, S.-M., Kim, E. A., Kim, J. Y., Kim, S., Yoo, J. S. & Park, Y. M. (2004). *J. Plant Physiol.* **161**, 837–845.
Kim, W. K., Lee, C. S. & Jeong, B. K. (1988). *J. Ginseng Res.* **12**, 93–103.
Kimura, Y., Schmitt, A., Fukushima, N., Ishii, I., Kimura, H., Nebreda, A. R. & Chun, J. (2001). *J. Biol. Chem.* **276**, 15208–15215.
Lee, J.-H., Choi, S.-H., Lee, B.-H., Hwang, S.-H., Kim, H.-J., Rhee, J., Chung, C. & Nah, S.-Y. (2013). *Neurosci. Lett.* **548**, 143–148.
Lytle, B. L., Song, J., de la Cruz, N. B., Peterson, F. C., Johnson, K. A., Bingman, C. A., Phillips, G. N. Jr & Volkman, B. F. (2009). *Proteins*, **76**, 237–243.
Marković-Housley, Z., Degano, M., Lamba, D., von Roepenack-Lahaye, E., Clemens, S., Susani, M., Ferreira, F., Scheiner, O. & Breiteneder, H. (2003). *J. Mol. Biol.* **325**, 123–133.
Mogensen, J. E., Wimmer, R., Larsen, J. N., Spangfort, M. D. & Otzen, D. E. (2002). *J. Biol. Chem.* **277**, 23684–23692.
Murshudov, G. N., Skubák, P., Lebedev, A. A., Pannu, N. S., Steiner, R. A., Nicholls, R. A., Winn, M. D., Long, F. & Vagin, A. A. (2011). *Acta Cryst.* D**67**, 355–367.
Neudecker, P., Schweimer, K., Nerkamp, J., Scheurer, S., Vieths, S., Sticht, H. & Rösch, P. (2001). *J. Biol. Chem.* **276**, 22756–22763.
Noguchi, K., Herr, D., Mutoh, T. & Chun, J. (2009). *Curr. Opin. Pharmacol.* **9**, 15–23.
Otwinowski, Z. & Minor, W. (1997). *Methods Enzymol.* **276**, 307–326.
Pagès, C., Simon, M.-F., Valet, P. & Saulnier-Blache, J. S. (2001). *Prostaglandins Other Lipid Mediat.* **64**, 1–10.
Pasternak, O., Bujacz, G. D., Fujimoto, Y., Hashimoto, Y., Jelen, F., Otlewski, J., Sikorski, M. M. & Jaskolski, M. (2006). *Plant Cell*, **18**, 2622–2634.
Pyo, M.-K., Choi, S.-H., Hwang, S.-H., Shin, T.-J., Lee, B.-H., Lee, S.-M., Lim, Y.-H., Kim, D.-H. & Nah, S.-Y. (2011). *J. Ginseng Res.* **35**, 92–103.
Radauer, C., Lackner, P. & Breiteneder, H. (2008). *BMC Evol. Biol.* **8**, 286.
Reitz, J., Gehrig-Burger, K., Strauss, J. F. III & Gimpl, G. (2008). *FEBS J.* **275**, 1790–1802.
Saraste, M., Sibbald, P. R. & Wittinghofer, A. (1990). *Trends Biochem. Sci.* **15**, 430–434.
Shin, T.-J., Kim, H.-J., Kwon, B.-J., Choi, S.-H., Kim, H.-B., Hwang, S.-H., Lee, B.-H., Lee, S.-M., Zukin, R. S., Park, J.-H., Kim, H.-C., Rhim, H., Lee, J.-H. & Nah, S.-Y. (2012). *Mol. Cells*, **34**, 563–572.
Sinha, M., Singh, R. P., Kushwaha, G. S., Iqbal, N., Singh, A., Kaushik, S., Kaur, P., Sharma, S. & Singh, T. P. (2014). *Sci. World J.* **2014**, 543195.
Sun, H., Kim, M.-K., Pulla, R. K., Kim, Y.-J. & Yang, D.-C. (2010). *Mol. Biol. Rep.* **37**, 2215–2222.
Sun, Y., Nam, J.-S., Han, D.-H., Kim, N.-H., Choi, H.-K., Lee, J. K., Rhee, H. J. & Huh, S.-O. (2010). *Cell. Signal.* **22**, 484–494.
Tigyi, G. & Miledi, R. (1992). *J. Biol. Chem.* **267**, 21360–21367.
Vagin, A. & Teplyakov, A. (2010). *Acta Cryst.* D**66**, 22–25.
Vogt, W. (1963). *Biochem. Pharmacol.* **12**, 415–420.
Webber, K. O. & Hajra, A. K. (1992). *Methods Enzymol.* **209**, 92–98.
Yanagida, K., Ishii, S., Hamano, F., Noguchi, K. & Shimizu, T. (2007). *J. Biol. Chem.* **282**, 5814–5824.